

Comparative study on the performance of serrated interfaces in multi-layer pavements

Ming-Jian Li^a, Xu-Dong Wang^b and Nian-Mei Zhang^{a*}

^a*School of Physics, University of Chinese Academy of Sciences, Beijing, People's Republic of China;*

^b*Research Institute of Highway, Ministry of Transport of China, Beijing, People's Republic of China*

(Received 31 August 2015; accepted 18 April 2016)

Bonding condition can significantly affect the performance of multi-layer asphalt pavements. This paper introduces a novel serrated interfaces design to enhance bonding condition between layers. Numerical studies on this model have been presented by using the non-linear finite element method. The multi-layer contact problem was solved by applying the Coulomb friction model and Lagrange multiplier methodology. To evaluate the performance of the serrated interfaces model, comparative studies with a fully bonded model and a smooth surface friction model have been conducted. Results suggest that the serrated interfaces model provides much more shear resistance than the smooth surface counterpart, and has similar performance as the ideal fully bonded model in terms of longitudinal and vertical displacements. Moreover, the serrated interfaces can change interfacial horizontal stresses into compressive ones, which is beneficial for preventing cracks at low temperature. Despite its limited effects on the reduction of vertical and shear stresses, the serrated interfaces should be a very promising development with appropriate designs and implementations.

Keywords: serrated interface; asphalt pavement; bonding condition; contact analysis; Lagrange multiplier method

1. Introduction

Bonding condition between layers is one of the most significant factors in the design of asphalt pavements. Traditional analysis usually assumes the multi-layer system as a monolithic structure without interfacial separation. However, bonding between layers in practice is often inadequate and contributes a lot to cracks, slippage, rutting and other failures. As the bonding problems have caused increasing concerns, several approaches have been carried out to extend the service life of pavements, for instance, the tack coat made with asphalt emulsion between asphalt layers or between asphalt and cement (Canestrari et al., 2013; Hachiya & Sato, 1997).

Due to the complexity and non-linearity of the analytical approach, experimental and numerical methods are most commonly applied to interfacial problems. Laboratory tests usually use tensile, shear, torque or wedge splitting to investigate and optimise the bonding condition (Raposeiras, Castro-Fresno, Vega-Zamanillo, & Rodriguez-Hernandez, 2013; Uzan, Livneh, & Eshed, 1978). Field investigations such as falling weight deflectometer (Hakim, Cheung, & Armitage, 2000) and accelerated testing programmes (Ozer, Al-Qadi, Wang, & Leng, 2012) have also been

*Corresponding author. Email: nmzhang@ucas.ac.cn

carried out for validation and back-calculation. Numerical analysis, especially finite element method (FEM), is widely used due to its effectiveness and high efficiency. Fully bonded models, fully slipped models and friction models have been extensively investigated. The Coulomb friction model and its improved models are commonly used (Kruncheva, Collop, & Thom, 2005; Romanoschi, 1999; Romanoschi & Metcalf, 2001; Yoo, Al-Qadi, Elseifi, & Janajreh, 2006). Most of these studies assume the interfaces between layers as a smooth plane. However, laboratory tests suggest that surface characteristics (surface roughness, macro and micro texture, contaminations and moisture) can significantly affect the bonding condition. Leng, Ozer, Al-Qadi, and Carpenter (2008) suggested that a transversely or longitudinally tined surface of Portland cement concrete (PCC) can increase interface shear strength when the tack coat application rate is low. A milled PCC surface can provide even larger interface shear strength with various tack coat application rates. Other studies (Santagata, Partl, Ferrotti, Canestrari, & Flisch, 2008; West, Zhang, & Moore, 2005) also found that rough or milled surfaces with grooving can lead to higher interface resistance than smooth surfaces.

2. Objectives and scope

Despite large numbers of studies on the friction model in the literature, it is difficult to find detailed numerical analysis for contact issues between rough or tined interfaces in pavements. Practically, the interfaces between hot-mix asphalt and PCC can be artificially tined or milled. For the design and construction of asphalt pavements, one possible way to increase interfacial bonding is to make transverse grooves on the lower layer surface. The longitudinal section thus becomes serrated. The serrated interfaces are expected to enhance the integrity of the pavement system. Since our laboratory and field investigations of this model are in progress, we focus mainly on numerical analysis in this paper. Here, serrated interfaces have been assumed in the model, and conducted a non-linear finite element contact analysis between pavement layers. Multi-layer pavements were modelled and compared with the traditional fully bonded model and smooth friction model.

3. Numerical methodology

3.1. Contact analysis methodologies

Contact analysis is widely used in mechanical engineering, civil engineering and other fields. Early finite element contact analysis can date back to direct iteration methods (Francavilla & Zienkiewicz, 1975). During iterating, the stiffness or flexibility matrix of the system should be regenerated. More common methodologies recently are Lagrange multiplier methods and penalty methods (Pantano & Averill, 2002; Tur, Fuenmayor, & Wriggers, 2009). Penalty methods introduce penalty parameters to approximate the boundary conditions. Contact constraint can thus be applied as variational inequalities in weak formulation. Theoretically, by choosing a rather large penalty parameter, the contact constraint tends to be accurately implemented. However, this will lead to ill-conditioned equations and the choice of penalty parameter becomes critical in calculation. On the other hand, the Lagrange multiplier method introduces Lagrange multipliers to exactly implement the contact constraint. In comparison between these two methods (Weyler, Oliver, Sain, & Cante, 2012), it is suggested both methods have similar performance when parameters are appropriately chosen. However, in some critical situations, the penalty method may lead to excessive penetration and thus produce undesired results. In this work, the Lagrange multiplier method is applied.

3.2. Lagrange multiplier method

3.2.1. Governing equations

For the contact problem between two bodies ${}^i\Omega$ ($i = 1, 2$) in Figure 1, ${}^i\Gamma$ are defined as their boundaries with normal vectors ${}^i\mathbf{n}$. The governing equations with boundary conditions can then be written as follows.

$$\text{Equilibrium equation : } \nabla \cdot {}^i\boldsymbol{\sigma} = {}^i\mathbf{b} \quad \text{in } {}^i\Omega, \tag{1}$$

$$\text{Constitutive equation : } {}^i\boldsymbol{\sigma} = {}^i\mathbf{D} : {}^i\boldsymbol{\varepsilon} \quad \text{in } {}^i\Omega, \tag{2}$$

$$\text{Geometric equation : } {}^i\boldsymbol{\varepsilon} = \frac{1}{2}[\nabla {}^i\mathbf{u} + (\nabla {}^i\mathbf{u})^T] \quad \text{in } {}^i\Omega, \tag{3}$$

$$\text{Dirichlet's boundary condition : } {}^i\mathbf{u} = {}^i\bar{\mathbf{u}} \quad \text{on } {}^i_D\Gamma, \tag{4}$$

$$\text{Neumann's boundary condition : } {}^i\boldsymbol{\sigma} \cdot {}^i\mathbf{n} = {}^i\bar{\mathbf{F}} \quad \text{on } {}^i_N\Gamma. \tag{5}$$

Herein $\boldsymbol{\sigma}$, $\boldsymbol{\varepsilon}$ and \mathbf{D} are stress, strain and elasticity tensors, respectively. \mathbf{b} and \mathbf{u} are body force and displacement vectors. $\bar{\mathbf{u}}$ and $\bar{\mathbf{F}}$ are pre-defined displacements and tractions on certain boundary areas.

3.2.2. Constraint implementation

Contact problems have additional boundary constraints. Define iF_n and ${}^iF_\tau$ as normal and tangential contact forces, and for a certain contact point pair we then have:

$${}^1F_n + {}^2F_n = 0, \quad {}^1F_\tau + {}^2F_\tau = 0. \tag{6}$$

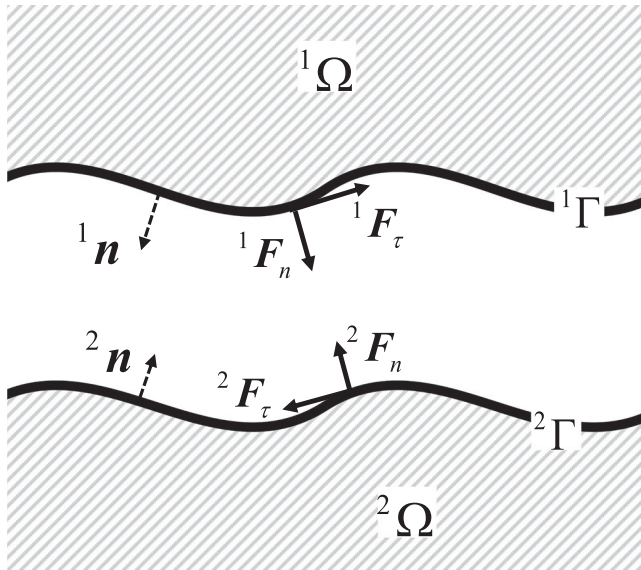


Figure 1. Contact model sketch.

Defining g_n as the minimum distance between two surfaces, the geometrical impenetrability condition can be described as follows with spatial coordinates ${}^i\mathbf{x}$

$$g_n = ({}^1\mathbf{x} - {}^2\mathbf{x}) \cdot {}^2\mathbf{n} \geq 0. \quad (7)$$

While interfacial cohesive forces are neglected, only pressure in the normal direction can be found. The normal traction condition can be described as follows:

$${}^i\mathbf{F}_n \leq 0. \quad (8)$$

In the Coulomb friction model, tangential forces can be described with friction coefficient μ :

$$|{}^i\mathbf{F}_\tau| \leq \mu |{}^i\mathbf{F}_n|. \quad (9)$$

The contact problems will be solved in procedures described in Figure 2, where ε_u is a small number for contact judgement, ${}^i_D\Gamma$, ${}^i_N\Gamma$ and ${}^i_C\Gamma$ are the prescribed Dirichlet, Neumann and possible contact boundaries. ${}^i\mathbf{u}_\tau$ and ${}^i\mathbf{u}_n$ denote tangential and normal interfacial displacement. BC means boundary conditions including the Dirichlet, Neumann and contact ones.

The functional of the system can be written as

$$\Pi = \Pi_P + \Pi_C \quad (10)$$

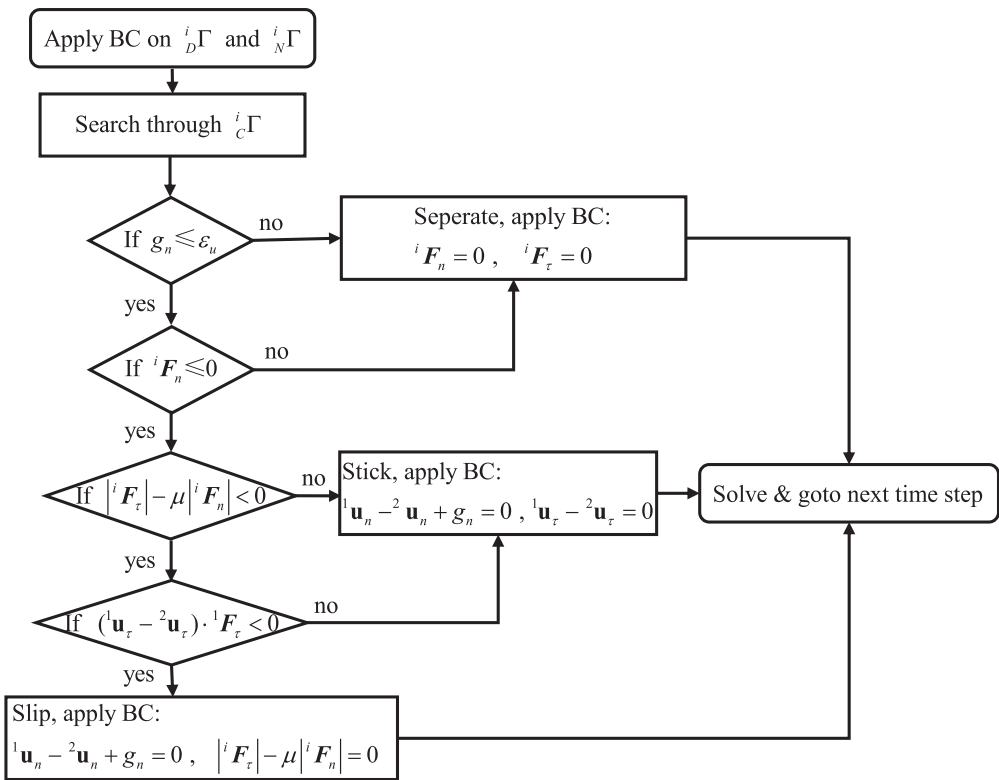


Figure 2. Flow chart of the contact problem algorithm.

with Π_P being the potential energy without contact constraint, and Π_C the additional contact functional. With Lagrange multiplier λ , it can be written as

$$\Pi_C = \int_{c\Gamma} [\lambda_n({}^1u_n - {}^2u_n + g_n) + \lambda_1({}^1u_1 - {}^2u_1) + \lambda_1({}^1u_2 - {}^2u_2)]dS. \quad (11)$$

By using the variational principle we have

$$\delta\Pi = \delta\Pi_P + \delta\Pi_C = 0. \quad (12)$$

We can then obtain the solution since only λ_n is independent and the impenetrability condition is applied here.

4. Modelling and numerical results

4.1. Geometry and material parameters

A six-layer model was established (Figure 3) in this work. Here, x , y and z are defined as longitudinal, vertical and transverse axes of the pavements, respectively. The origin is located at the centre of the load on the surface of the road. All six layers have serrated interfaces in-between. h and θ are the height and angle of these serrations, and here $h = 0.01\text{m}$ and $\theta = 90^\circ$. The traffic loads on the road surface include vertical and horizontal loads. Tyre pressure is 707 kPa according to the Chinese BZZ-100 standard, and its contact length is set to be 0.22 m. Horizontal load is defined as 0.7 times the magnitude of vertical load for simulating a typical sudden brake case on a dry, clean asphalt road. Both loads are distributed uniformly.

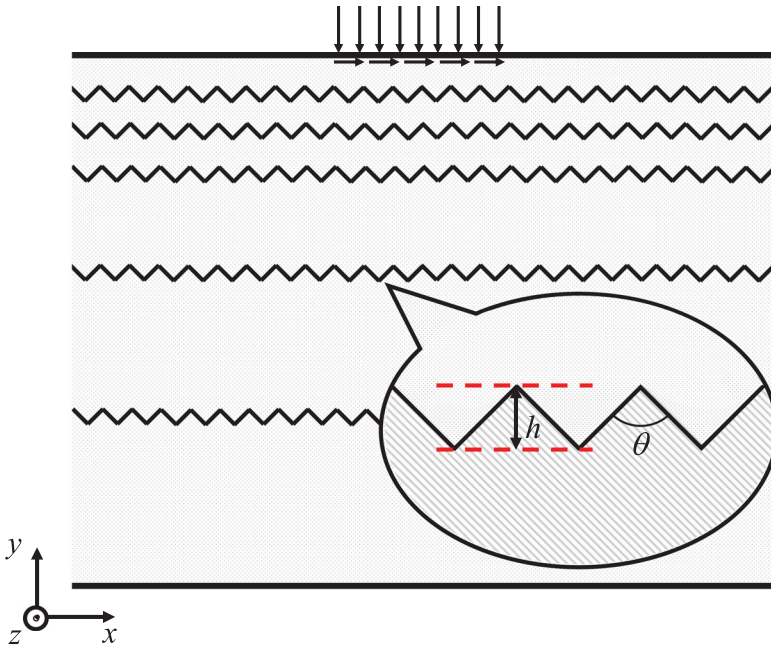


Figure 3. Geometry of multi-layer pavements with serrated interfaces.

Table 1. Material parameters of each layer.

Layer	Material	Thickness (m)	Elastic modulus (MPa)	Poisson's ratio
Asphalt layers	Fine-grained asphalt concrete	0.04	1400	0.3
	Medium-grained asphalt concrete	0.05	1200	0.3
	Medium-grained asphalt concrete	0.06	1200	0.3
Base	Cement stabilised macadam	0.20	1700	0.25
Subbase	Limestone soil	0.40	550	0.3
Subgrade	Soil	0.40	45	0.3

The material parameters of each layer are listed in Table 1. The choice of materials is based on a typical design and the recommendations of Chinese standard (Ministry of transport of China, 2006) on asphalt pavements. All materials are considered as linear elastic and isotropic here. The typical pavement temperature here is 20°C.

4.2. Validation of algorithm and model

4.2.1. Analytical approach validation and grid independence test

Since field and laboratory investigations for the serrated interface model are quite difficult to find, two validating cases considering an analytical solution and grid independence verification have been presented here.

The classic semi-infinite elastic problem can be applied to validate a simple road model. In a semi-infinite elastic body under circular uniform pressure p with a radius of δ , the vertical displacement w and vertical stress σ_z can be written in the following form:

$$w = \frac{(1 + \mu)p\delta}{E} \int_0^\infty \left(2 - 2\mu + \frac{z}{\delta}x\right) e^{-(z/\delta)x} \frac{J_1(x)J_0\left(\frac{r}{\delta}x\right)}{x} dx, \quad (13)$$

$$\sigma_z = -p \int_0^\infty \left(1 + \frac{z}{\delta}x\right) e^{-(z/\delta)x} J_1(x)J_0\left(\frac{r}{\delta}x\right) dx. \quad (14)$$

Here, E and μ are elastic modulus and Poisson's ratio. z and r are vertical and radial coordinates, and $x = \xi\delta$. J denotes the Hankel transform function. The vertical displacement and stress on the

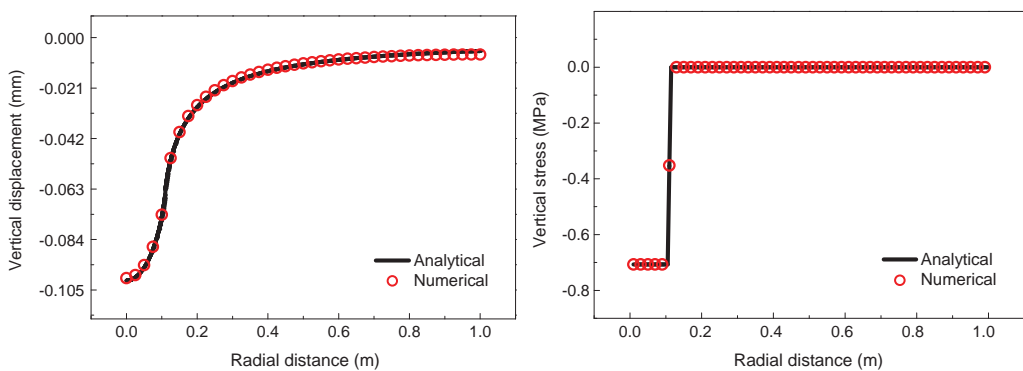


Figure 4. Validation with the semi-infinite elastic model – vertical displacement and stress for the surface of the road.

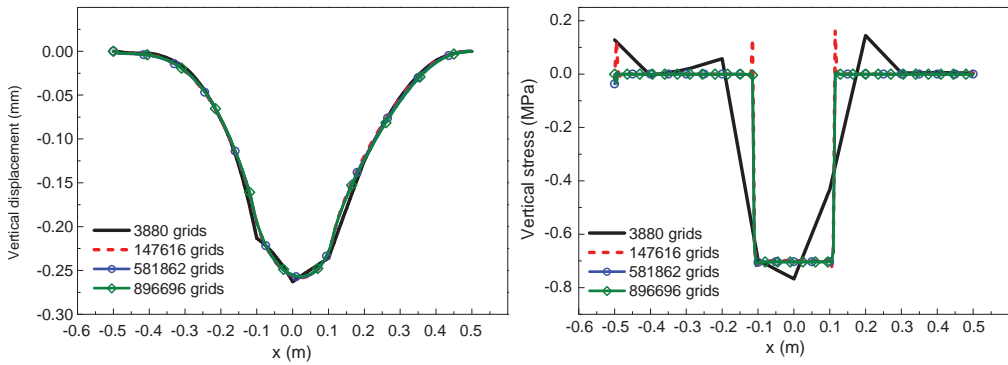


Figure 5. Grid independence verification of the model.

road surface ($z = 0$) calculated by the FE model have been validated with the analytical solution. Figure 4 shows good agreement between the FE approach and the analytical approach.

The grid independence verification case was then carried out. The six-layer serrated interface model was calculated with various spatial discretisation forms. Figure 5 suggests that with

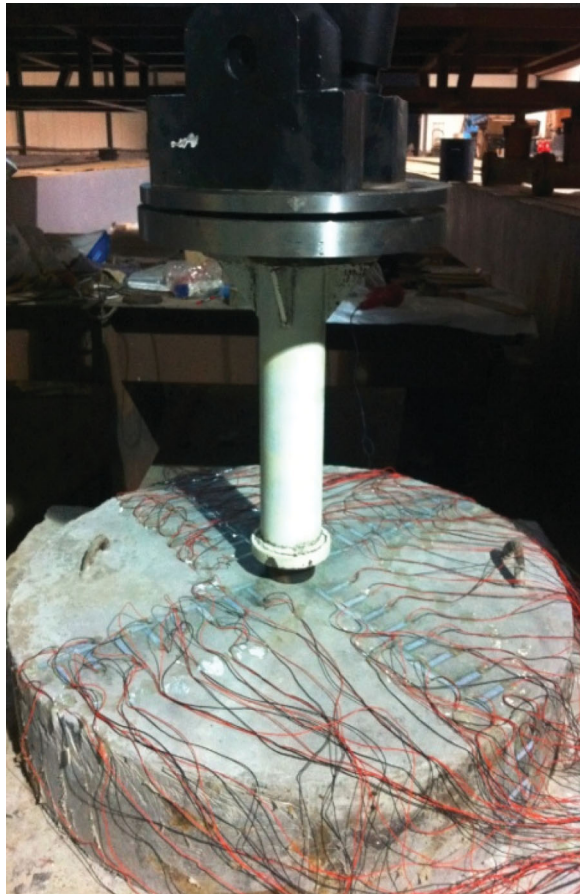


Figure 6. Experiment on a cement disc under pressure.

fine enough grids, the numerical solution will be grid independent. The numerical model with appropriate discretisation will then be applied in the following part.

4.2.2. Laboratory tests verification

Here, a model with one layer has been verified with laboratory tests. A cement thick disc with a diameter 1 m and thickness 20 cm has been made. A uniformly distributed pressure from 2.3 to 2.9 MPa has been applied to the centre of the surface. The steel cylinder for load application has a diameter of 15 cm. More than 30 strain gauges have been installed on the surface of the cement disc. Radial and tangential strains at different locations have been tested under different pressures. Experiments have been carried out for more than 20 times for each load level and the average strains have been compared with those were calculated with the FE model. An elastic modulus of 30,000 MPa and a Poisson’s ratio of 0.3 have been set during the calculation (Figure 6).

It can be seen from Figure 7 that the FE calculation in the one-layer cement model has good agreement with the experimental results in most areas. Since the strain gauge installed too near the load centre may be damaged, the strains in these areas are not available. Although the one-layer model is different from the serrated model, the basic FE calculation process can be verified through this case.

4.3. Comparative studies on multi-layer pavements

In order to evaluate the mechanical performance of the multi-layer model with serrated interfaces (hereinafter the “serrated model”), two additional models have been investigated for comparison.

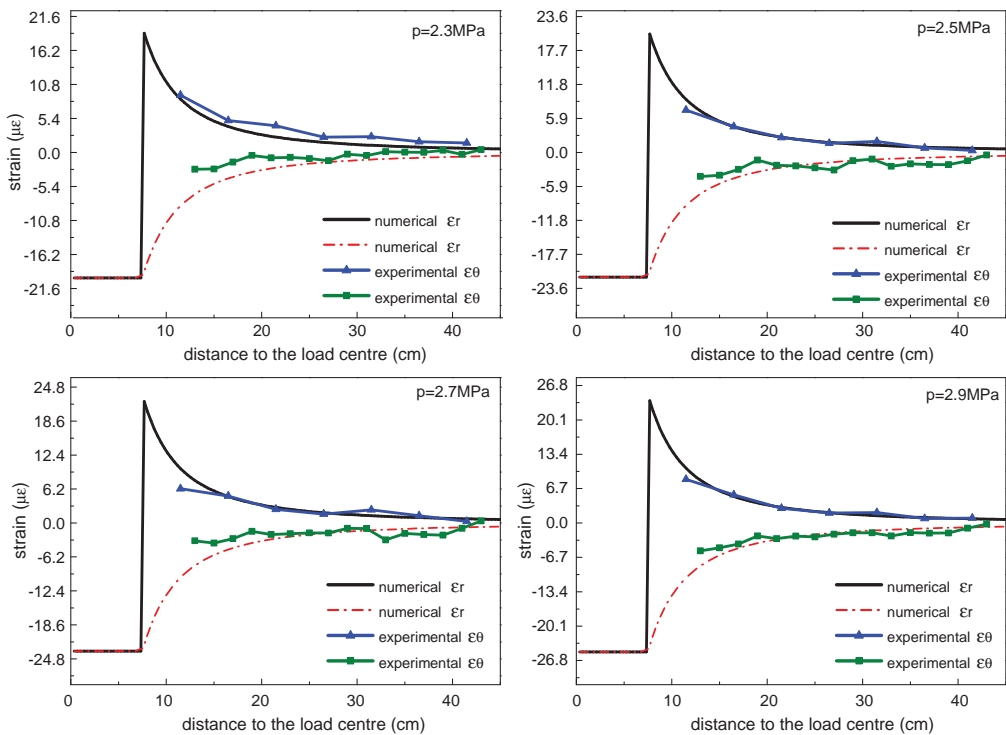


Figure 7. Comparison between numerical and experimental results for radial and tangential strains.

One is a fully bonded model which has continuous displacement between layers (the “continuous model” for short), and the other one is a Coulomb friction model with smooth interfaces between layers (the “smooth model” or “smooth friction model”). The friction coefficient of the smooth model is 0.7 which is the same as the serrated model. Comparative studies on these models are presented in the following part.

4.3.1. Displacement comparison

Figure 8 displays the displacement distribution of the serrated model, and the most interesting feature of this contour is the discontinuity of interfacial displacement. In both the smooth and the serrated models, interfacial separation can be found in longitudinal and vertical directions. The detailed view with 200 times amplification presents this feature clearly, especially in the region behind the wheel. Due to the continuity of material, the upper layers will be lifted up slightly under the traffic loads. Although the magnitude of displacements is rather small, the tendency of separation truly exists.

Here, we focus on investigation of the most critical areas of the multi-layer system, including the surface of the asphalt layer and all five interfaces. The displacements and stresses of these areas along the longitudinal direction are presented in the following figures in the order of their depths.

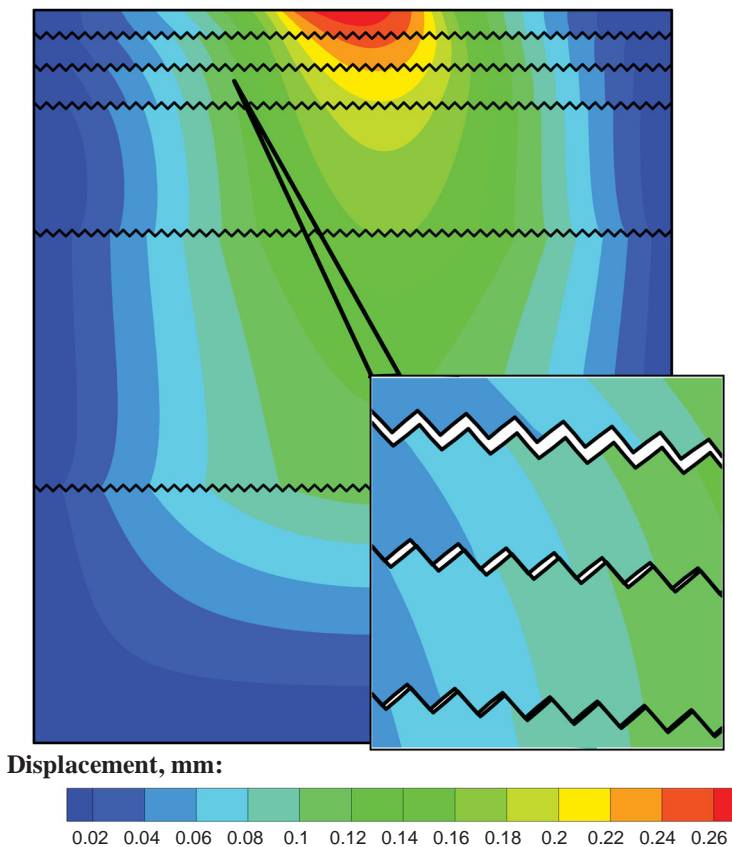


Figure 8. Displacement distribution and interfacial details.

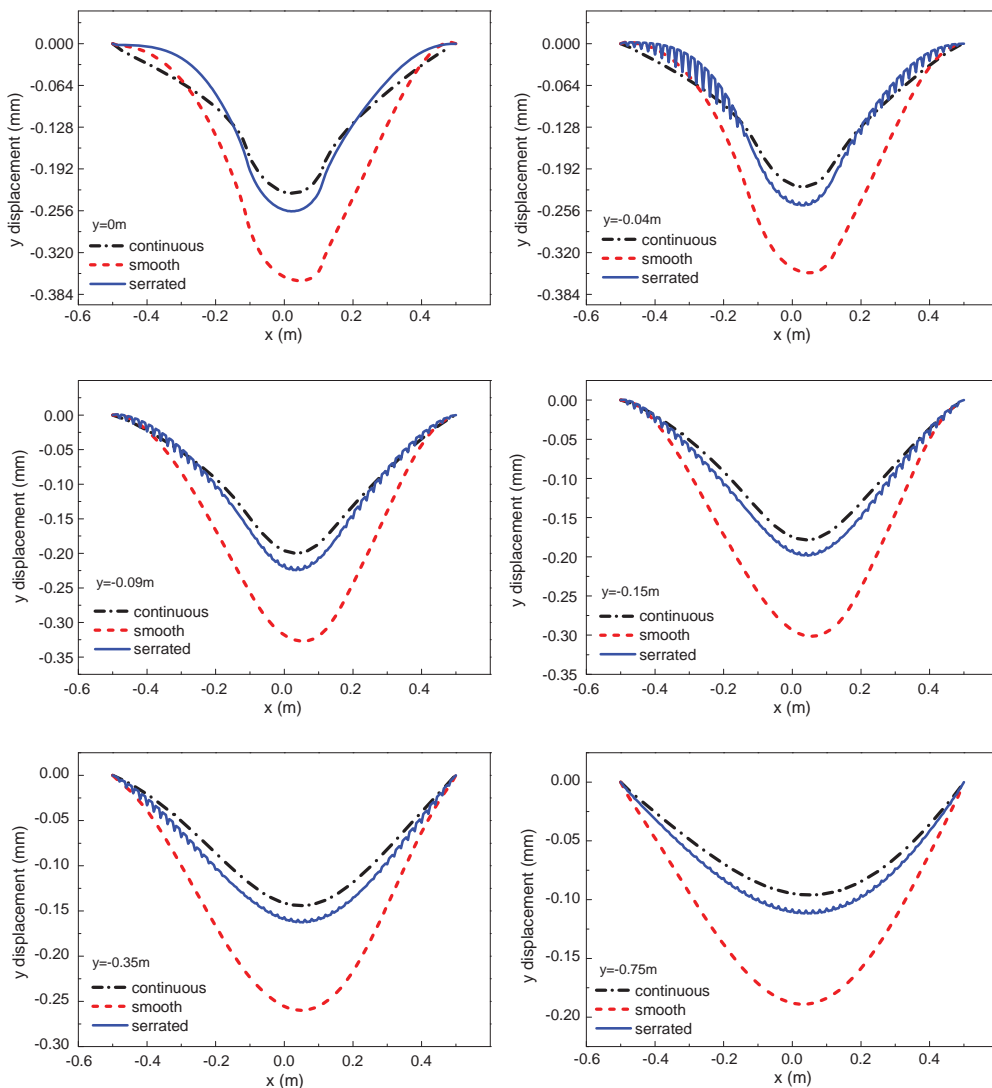


Figure 9. Vertical displacements at different depths.

The vertical displacements of all three models are displayed in Figure 9. As can be seen, the serrated model leads to larger displacement than the continuous one; however, it apparently improves the bonding condition compared with the smooth model. On the surface of the asphalt layer, maximum vertical displacement of the serrated model is 12% larger than that of the continuous one and 29% smaller than that of the smooth model. As the depth increases, displacements of all models decrease, and the vertical displacements of the serrated model are always smaller than those of the smooth model.

The horizontal slippage under traffic loads is significantly influenced by the bonding condition. Figure 10 shows that the smooth model causes the largest longitudinal displacement on each interfaces. The serrated model, however, can greatly reduce the horizontal displacement, especially on interfaces at $y = -0.04$ and $y = -0.09$ m. Considering horizontal slippage

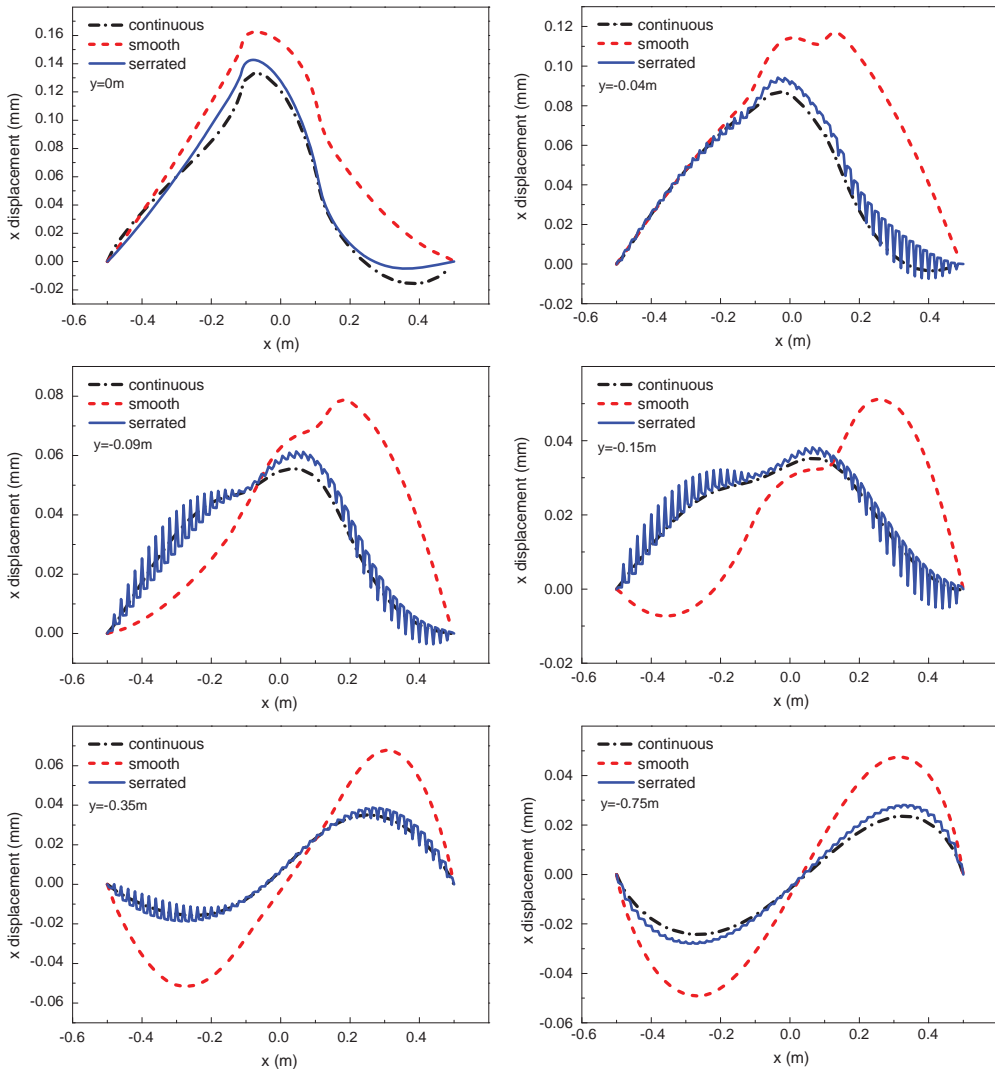


Figure 10. Longitudinal displacements at different depths.

prevention, the performance of the serrated model is quite close to the continuous one, and is much better than the smooth model.

4.3.2. Interfacial stresses comparison

Various stresses for all three models are presented here to further evaluate the performance of different pavement systems.

The vertical stresses on each interface are presented in Figure 11. On the road surface, the vertical stresses are basically the same as the imposed traffic loads. As the depth increases, the maximum vertical stress of the serrated model can be slightly smaller than that of the smooth model. On interfaces between layers with different modulus, the vertical stresses fluctuate in the longitudinal direction due to the geometrical characteristics. As a consequence, the effect on vertical stress reduction of the serrated model is very limited.

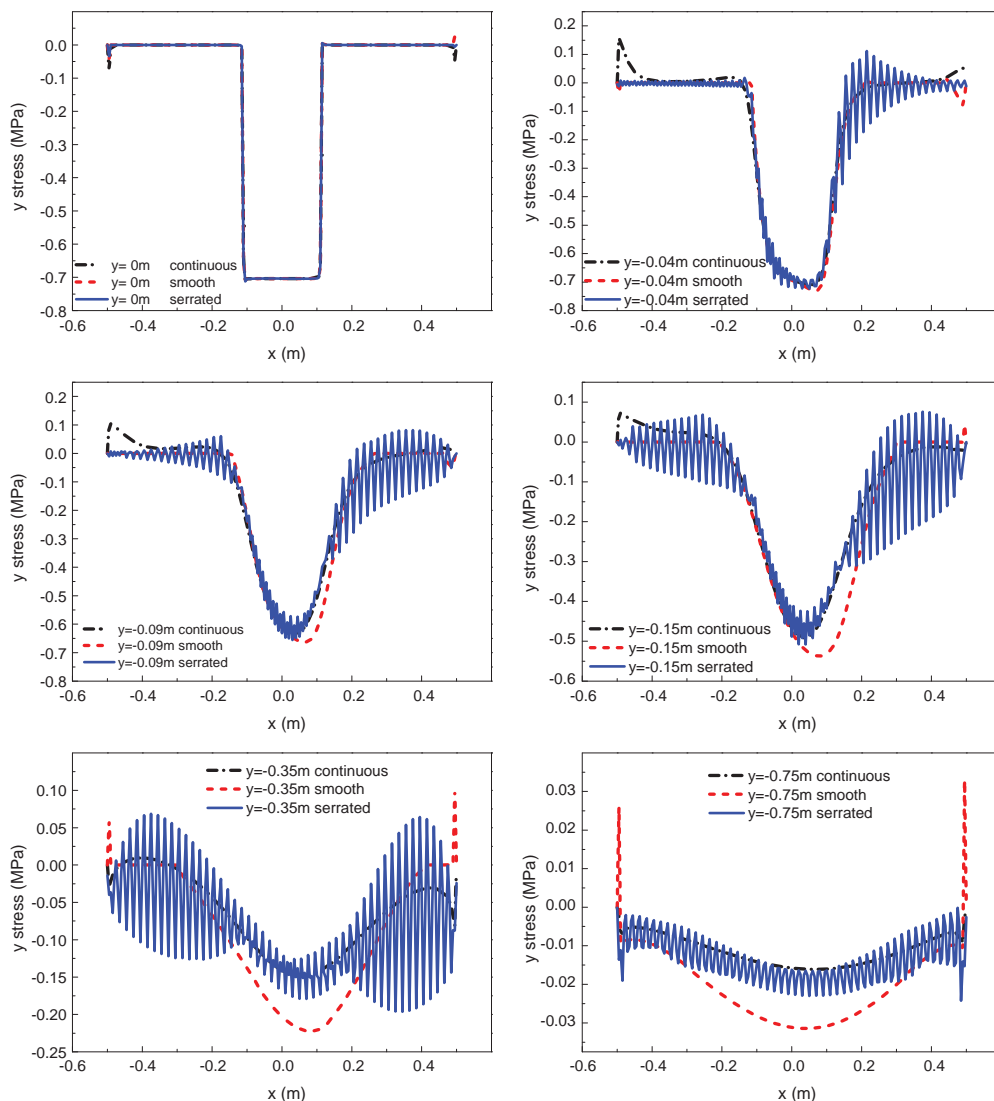


Figure 11. Vertical stresses at different depths.

The horizontal tensile stresses can cause cracks in pavements, especially at low temperature. Figure 12 shows longitudinal stresses at different depths. The stresses on the road surface are similar for all three models. However, very different features on the lower interfaces can be found. In the continuous model, the horizontal load typically causes compressive stress in the same direction as that of the horizontal force and tensile stress in the opposite direction. The smooth model has even larger tensile stresses. However, the serrated model suffers almost no tensile stresses beneath the road surface. The compressive stresses are also smaller in most areas compared with the other two models. The reason is that the serrations will separate from each other (Figure 8) under tensile stresses and will mainly cause compressive stresses. This unique feature of the serrated model is quite beneficial for the prevention of cracks at low temperature.

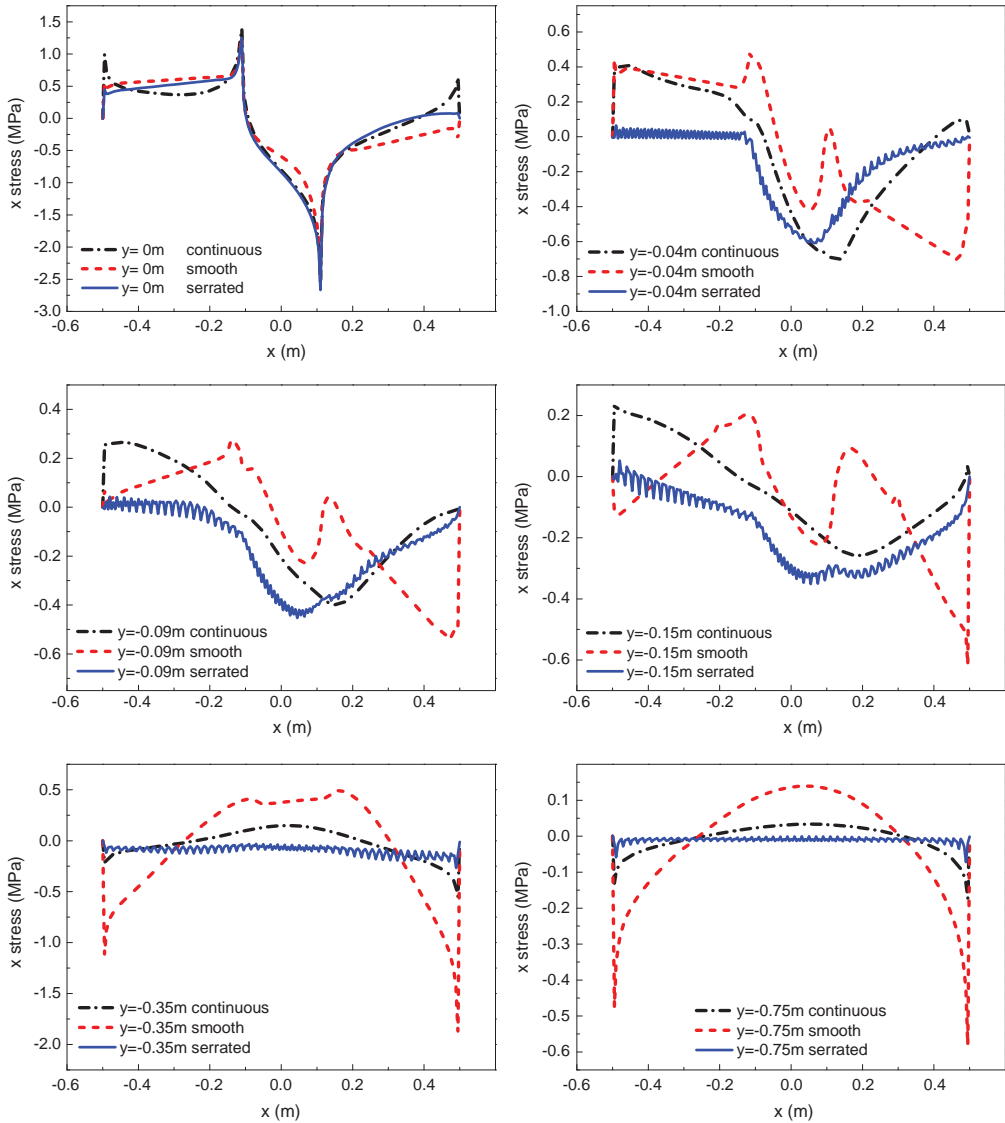


Figure 12. Longitudinal stresses at different depths.

Shear failure is another important factor to be considered. Figure 13 shows that the shear stresses of the serrated model are similar to those of the continuous model on upper interfaces, but the shear stresses are larger and are more fluctuated than those of the other two models on other interfaces. In this sense, the serrated model is not promising for the prevention of shear failures in pavements.

Figure 14 suggests that the von Mises stresses of three models are similar on the road surface. When the depth increases, the serrated model will have similar stresses to the continuous model. Especially with $y = -0.75$ m, the von Mises stresses of the serrated model are even smaller than for the continuous model.

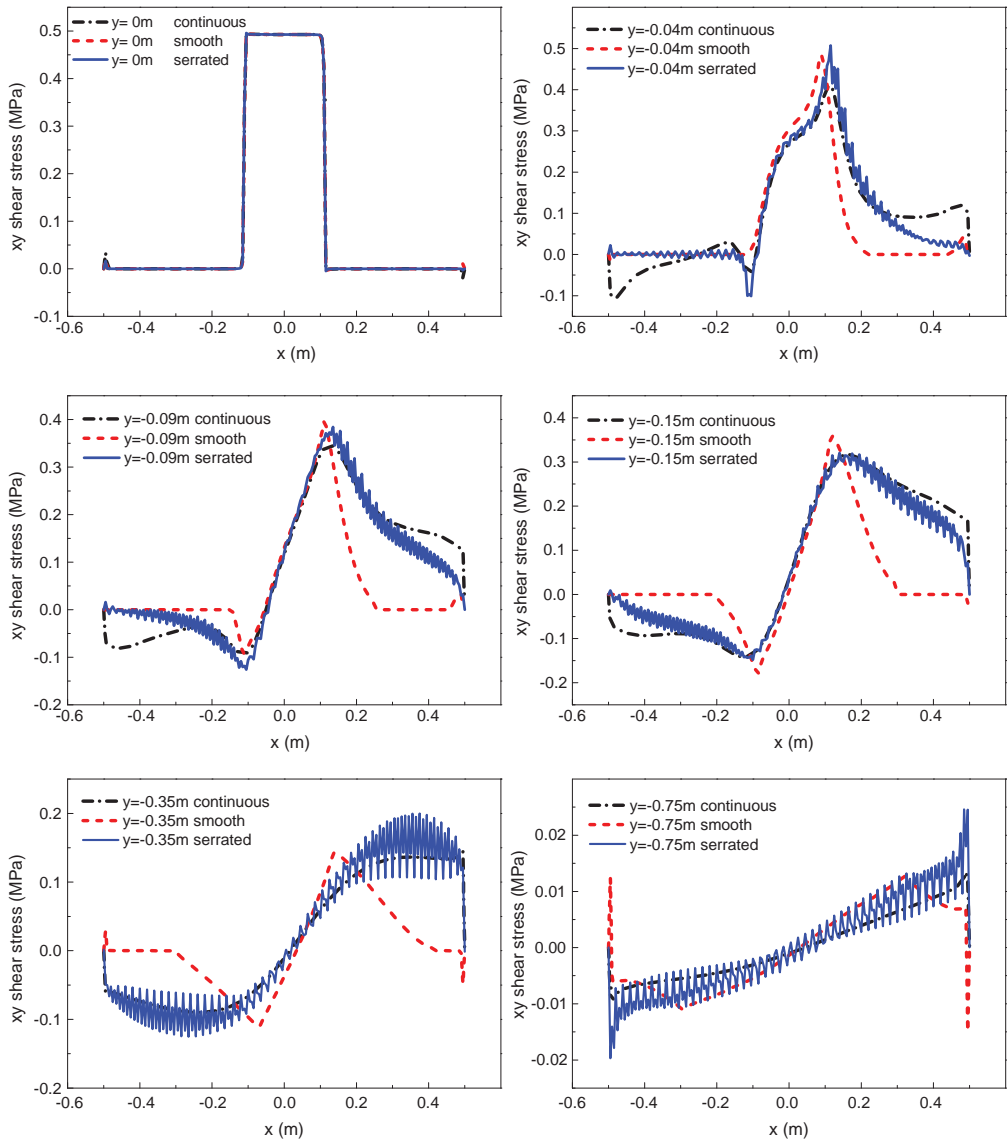


Figure 13. Shear stresses at different depths.

It can be seen from the discussions above that the serrated interface may cause larger stress in some areas. This is because the pointed edges of the serrated interface will lead to stress concentration and bring potential material failure problems.

5. Conclusions and discussion

For improvement of the interfacial bonding condition, the serrated interfaces model has been introduced. To study its effectiveness and mechanism, the Lagrange multiplier method was applied in finite element contact analysis. Comparative studies with a fully bonded model and a smooth friction model suggest that the serrated model has several unique features and is quite

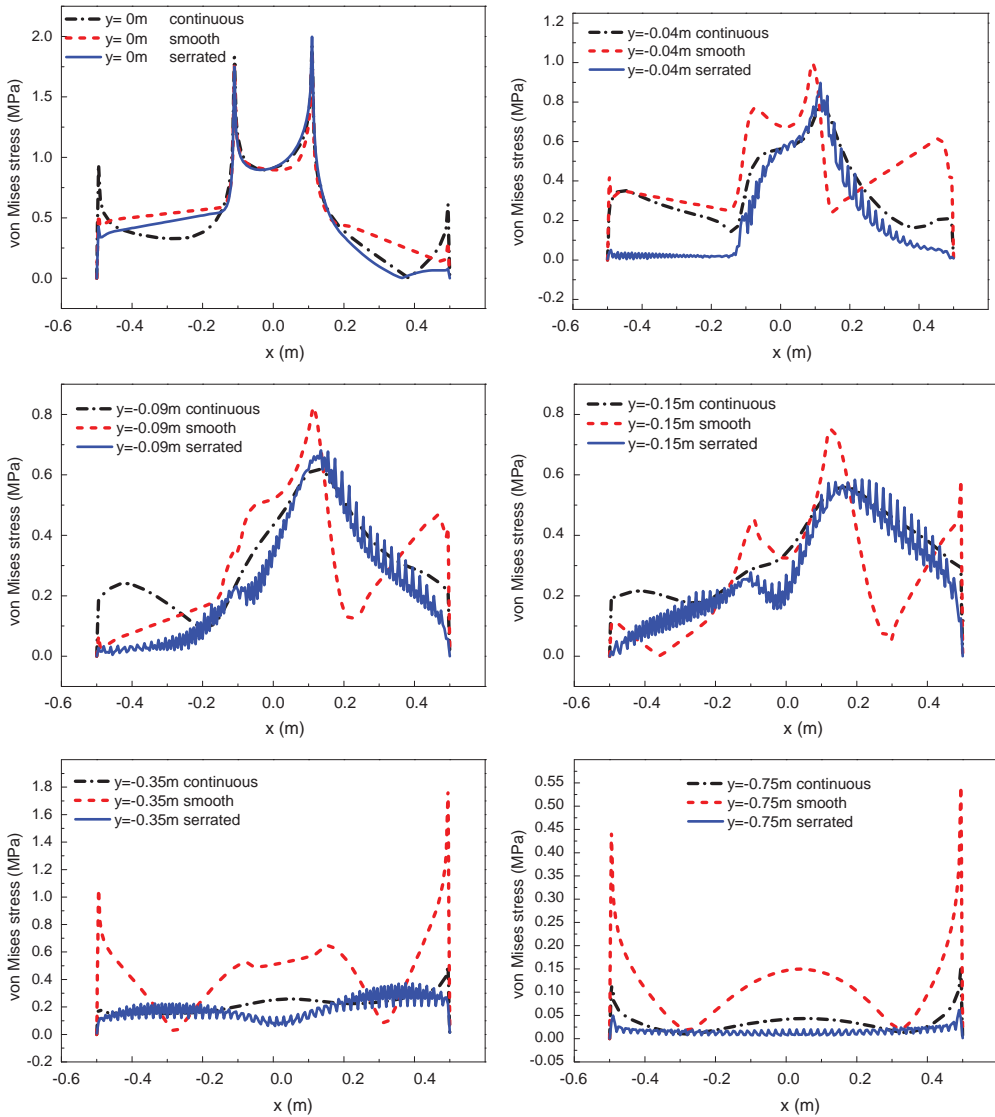


Figure 14. Equivalent stresses at different depths.

promising in many aspects. These findings from results and analysis above are summarised as follows:

- (1) Compared with the smooth friction model, the serrated model can significantly reduce the horizontal displacements on each interface, and its performance is quite close to the continuous model. The serrated model can also reduce vertical displacements compared with the smooth friction model.
- (2) Since the serrations can separate from each other, the serrated model bears mainly compressive stresses in the longitudinal direction on each interface. The lack of tensile stresses is very beneficial for preventing the generation and propagation of cracks at low

temperature. In this aspect, the serrated model performs better than both the continuous and the smooth friction model.

- (3) The serrated model has very limited effect on the reduction of vertical stresses. Moreover, the large and fluctuated interfacial shear stresses means that this model is not promising for preventing shear failures.

The serrated model is quite promising especially in horizontal displacement reduction and tensile stress prevention. It can improve the continuity of the pavement and better prevent cracks, rutting and slippage according to the numerical results. However, due to its complexity and non-linearity, this problem still needs more field and laboratory verification. Also, potential additional difficulties and higher prices in the construction and maintenance process should be noticed. More comprehensive work is expected in this interesting and promising direction.

Disclosure statement

No potential conflict of interest was reported by the authors.

References

- Canestrari, F., Ferrotti, G., Lu, X., Millien, A., Partl, M. N., Petit, C., ... Raab, C. (2013). *Mechanical testing of interlayer bonding in Asphalt pavements*. Dordrecht, Netherlands: Springer.
- Francavilla, A., & Zienkiewicz, O. (1975). A note on numerical computation of elastic contact problems. *International Journal for Numerical Methods in Engineering*, 9(4), 913–924.
- Hachiya, Y., & Sato, K. (1997). Effect of tack coat on binding characteristics at interface between asphalt concrete layers. *Proceedings of 8th International Conference on Asphalt Pavements, 1*, 349–362.
- Hakim, B. A., Cheung, L. W., & Armitage, R. J. (2000). Use of FWD data for prediction of bonding between pavement layers. *International Journal of Pavement Engineering*, 1(1), 49–59.
- Kruntcheva, M. R., Collop, A. C., & Thom, N. H. (2005). Effect of bond condition on flexible pavement performance. *Journal of Transportation Engineering*, 131(11), 880–888.
- Leng, Z., Ozer, H., Al-Qadi, I. L., & Carpenter, S. H. (2008). Interface bonding between hot-mix asphalt and various Portland cement concrete surfaces. *Transportation Research Record*, 11(2057), 46–53.
- Ministry of transport of China. (2006). Specifications for design of highway asphalt pavement JTGD50-2006 (in Chinese).
- Ozer, H., Al-Qadi, I. L., Wang, H., & Leng, Z. (2012). Characterisation of interface bonding between hot-mix asphalt overlay and concrete pavements: Modelling and in-situ response to accelerated loading. *International Journal of Pavement Engineering*, 13(2), 181–196. doi:10.1080/10298436.2011.596935
- Pantano, A., & Averill, R. C. (2002). A penalty-based finite element interface technology. *Computers & Structures*, 80(22), 1725–1748.
- Raposeiras, A. C., Castro-Fresno, D., Vega-Zamanillo, A., & Rodriguez-Hernandez, J. (2013). Test methods and influential factors for analysis of bonding between bituminous pavement layers. *Construction and Building Materials*, 43, 372–381. doi:10.1016/j.conbuildmat.2013.02.011
- Romanoschi, S. A. (1999). *Characterization of pavement layer interfaces (Ph.D)*. Louisiana State University and Agricultural & Mechanical College.
- Romanoschi, S. A., & Metcalf, J. B. (2001). Characterization of asphalt concrete layer interfaces. *Transportation Research Record*, 1778, 132–139.
- Santagata, F., Partl, M., Ferrotti, G., Canestrari, F., & Flisch, A. (2008). Layer characteristics affecting interlayer shear resistance in flexible pavements. *Proceedings of Association of Asphalt Paving Technologists*, 77, 221–256.
- Tur, M., Fuenmayor, F., & Wriggers, P. (2009). A mortar-based frictional contact formulation for large deformations using Lagrange multipliers. *Computer Methods in Applied Mechanics and Engineering*, 198(37), 2860–2873.
- Uzan, J., Livneh, M., & Eshed, Y. (1978). Investigation of adhesion properties between asphaltic-concrete layers. *Proceedings of the Association of Asphalt Paving Technologists, Technical Sessions*, 47, 495–521.

- West, R. C., Zhang, J., & Moore, J. (2005). Evaluation of bond strength between pavement layers. *NCAT Report*, 05-08.
- Weyler, R., Oliver, J., Sain, T., & Cante, J. C. (2012). On the contact domain method: A comparison of penalty and Lagrange multiplier implementations. *Computer Methods in Applied Mechanics and Engineering*, 205–208, 68–82. doi:10.1016/j.cma.2011.01.011
- Yoo, P. J., Al-Qadi, I. L., Elseifi, M. A., & Janajreh, I. (2006). Flexible pavement responses to different loading amplitudes considering layer interface condition and lateral shear forces. *International Journal of Pavement Engineering*, 7(1), 73–86. doi:10.1080/10298430500516074